Integrated Pressure Sensing Using Capacitive Coriolis Mass Flow Sensors

Dennis Alveringh, Remco J. Wiegerink, and Joost C. Lötters

***Abstract*— The cross-sectional shape of microchannels is, dependent on the fabrication method, never perfectly circular. Consequently, the channels deform with the pressure, which is a non-ideal effect in flow sensors, but may be used for pressure sensing. Multiple suspended channels with different lengths were modeled, fabricated, and characterized to verify the use and the scalability of this effect for pressure sensing. Furthermore, it is shown that the pressure dependence can be distinguished from the Coriolis effect in microfabricated Coriolis mass flow sensors, enabling the measurement of the pressure next to flow and density with only the flow sensor itself. In addition, this allows for further improvement in the accuracy of the flow measurement by correcting for the small pressure dependence. [2016-0236]**

***Index Terms*— Pressure sensing, Coriolis flow sensor, multi parameter system, differential pressure flow sensing, microfluidics, surface channel technology.**

I. Introduction

SENSING fluidic parameters has numerous applications in industry and healthcare [1]. The miniaturization of the sensors using microfabrication has advantages for most applications, e.g. higher sensitivities and lower unit prices [1], [2]. Different fabrication methods are available in microtechnology and different materials can be used as channel material. Further more, integration of multiple sensors on one chip is possible without increasing the costs or complexity and makes multi parameter sensing possible, which enables the measurement of e.g. the viscosity and density of the fluid [3], [4].

Disadvantages are also involved with microfabricated channels. Many fabrication methods for micro channels, made of e.g. PDMS [5], SU-8 [6], silicon [7] or silicon nitride [8], [9] are not circular as is illustrated in Figure 1. Non ideal effects when using the channels are self-evident, like: dead volumes, complicated flow patterns and pressure dependent deformation of the structures. The non-circularly shapes as described in the references are often inherent to the fabrication process and not easily solved without radical changes to the fabrication method.

Manuscript received September 30, 2016; revised February 24, 2017; accepted March 25, 2017. Date of publication April 13, 2017; date of current version May 31, 2017. This work was supported by the Eurostars Programme through the TIPICAL Project under Grant E!8264. Subject Editor J. Brugger. *(Corresponding Author: Dennis Alveringh.)*

D. Alveringh and R. J. Wiegerink are with the MESA+ Institute for Nanotechnology, University of Twente, 7500 AE Enschede, The Netherlands. (e-mail: d.alveringh@utwente.nl).

J. C. Lötters is with the MESA+ Institute for Nanotechnology, University of Twente, 7500 AE Enschede, The Netherlands, and is also with Bronkhorst High-Tech BV, 7261 AK Ruurlo, The Netherlands.

Color versions of one or more of the figures in this paper are available online at http://ieeexplore.ieee.org.

Digital Object Identifier 10.1109/JMEMS.2017.2689162

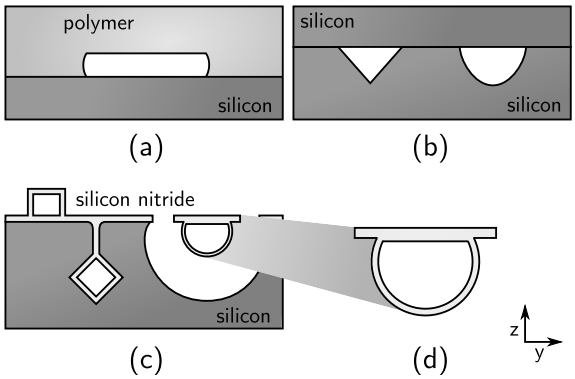

Fig. 1. Artist's impression of multiple non-circularly shaped micro channels, with (a) PDMS or SU-8 channels bonded on silicon [5], [6], (b) etched channels in silicon bonded on silicon [7], (c) channels of silicon nitride on or in silicon [8]–[10] and (d) close-up of the cross-section of a (suspended) surface channel.

The surface channel technology, comprehensively described in [10], has the same non-ideal effect. A cross-section of the channel is illustrated in Figure 1d. These channels are used in several fluid sensors, e.g. thermal flow sensors [11], Coriolis mass flow sensors [12] and pressure sensors [8], [13]. In latter sensors, the non-circularly shape plays, due to its pressure dependence, a crucial role in the transduction principle. The channel deforms due to pressure, which can be detected by e.g. change in displacement or resonance frequency.

In this article, we describe how the non-circular surface channels can be used to measure pressure and how pressure sensing can be implemented in a Coriolis mass flow sensor without changing the sensor design. This enables the Coriolis mass flow sensor to measure pressure as well as mass flow and density. The article is organized as follows. First, in Section II, we will explain the pressure sensing mechanism. Next, in Section III, we will show how this mechanism can be used in existing micro Coriolis mass flow sensors. In Section IV, we will discuss the fabrication process that was used to fabricate test devices. Measurement results are presented in Section V, followed by a discussion and conclusion.

II. Pressure Sensing

The non-circularly shaped channel pressure sensor is based on the asymmetry of the stiffness between the upper and lower part of the suspended channel as presented in [13]. The pressure in the channel causes a force on the walls. The forces cancel eachother around the channel, except for the tip, where the pressure results in a net longitudinal force. The asymmetry causes the channel to bend upwards, this can be detected by a change in capacitance as is illustrated in Figure 2.

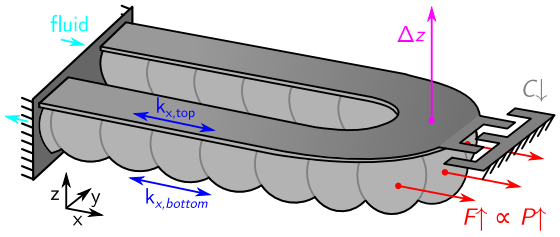

Fig. 2. The asymmetry of the channel's cross-section (Figure 1d) causes a variation in stiffness along z-direction, forcing it to deform under pressure. The electrodes at the tip enable capacitive readout.

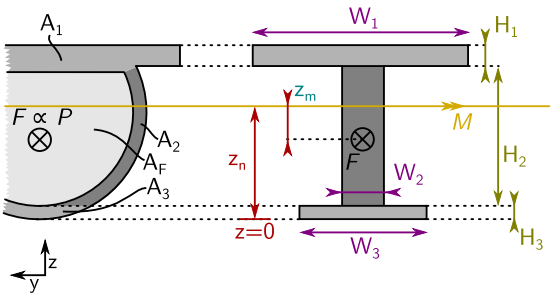

Fig. 3. Cross-section of the channel and its equivalent I-beam model with the definition of the dimensions.

A. Analytical Model

The mechanics are analyzed using a more accurate model than described in [13]. Modeling of the tube in Figure 2 is done by applying two simplifications.

- Only half (one part of the pair) of the U-shaped tube is modeled as a straight tube, since the full pair has twice the stiffness but also twice the force at the tip, which results in the same displacement.
- The complicated channel section is divided in three parts: the ceiling, the tube walls and the floor. The three parts are simplified to an asymmetric I-beam, as is illustrated in Figure 3.

The asymmetric I-beam will be analyzed by first defining the geometry, including the absolute centers and the neutral axes. Then, a net moment will be derived from the longitudinal force on the asymmetric I-beam. Finally, the second moments of area will be derived and used in combination with the net moment to find the displacement at the tip.

The three solid surfaces, A_1, A_2 and A_3, have the following area:

$$A_i = W_i H_i, \tag{1}$$

with W_i and H_i the width and height of surface area i respectively. These surfaces have absolute centers $z_{c,i}$:

$$z_{c,1} = H_3 + H_2 + \left(\frac{H_1}{2}\right), \tag{2}$$

$$z_{c,2} = H_3 + \left(\frac{H_2}{2}\right), \tag{3}$$

$$z_{c,3} = \left(\frac{H_3}{2}\right). \tag{4}$$

TABLE I
DIMENSIONS AND CONSTANTS FOR THE MODEL

W_1	60 µm
W_2	$2 \cdot 0.5$ µm
W_3	9 µm
H_1	3.6 µm
H_2	37 µm
H_3	0.5 µm
z_0	3.5 µm
L_0	1000 µm ... 2500 µm
A_F	1400 µm^2
E	295 GPa

The neutral axis z_n is defined as the axis through the I-beam where the stresses and strains are zero. Therefore, it passes through the centroid. The z-coordinate z_n can be found by the above defined absolute centers and the surface areas of the parts [14]:

$$z_n = \frac{z_{c,1}A_1 + z_{c,2}A_2 + z_{c,3}A_3}{A_1 + A_2 + A_3}. \tag{5}$$

The channel deforms as a result of the moment M caused by the net force F due to the pressure P and the distance z_m between the neutral axis z_n and the point on which the force acts (in the centroid of surface A_f, approximated by $z_{c,2}$):

$$M(P) = F(P)\, z_m = P\, A_F\, z_m = P\, A_F\, (z_n - z_{c,2}), \tag{6}$$

with A_F the surface area on which the pressure acts.

From the Huygens-Steiner theorem [14], the second moments of area I_i can be derived for the three parts.

$$I_1 = \frac{1}{12} W_1 H_1^3 + A_1 (z_1 - z_n)^2, \tag{7}$$

$$I_2 = \frac{1}{12} W_2 H_2^3 + A_2 (z_n - z_2)^2, \tag{8}$$

$$I_3 = \frac{1}{12} W_3 H_3^3 + A_3 (z_n - z_3)^2. \tag{9}$$

The sum

$$I = \sum I_i = I_1 + I_2 + I_3 \tag{10}$$

is the moment of inertia of the I-beam. A derivative of the beam theory of Euler-Bernoulli states that moment M, the Young's modulus E, the moment of inertia I and the displacement $\Delta z(x)$ are related:

$$M(P) = -EI \frac{d^2 \Delta z(x)}{dx^2}, \tag{11}$$

or, rewritten to find the displacement at the tip:

$$\Delta z(P) = \int_0^{L_0} \int \frac{M(P)}{EI}\, dx dx = \frac{M(P) L_0^2}{2EI}, \tag{12}$$

with L_0 the length of the I-beam.

The dimensions and constants can be found in Table I. Inner surface area A_F is derived from a microscope image of a section of the channel, the Young's modulus E for silicon rich nitride is taken from literature [15].

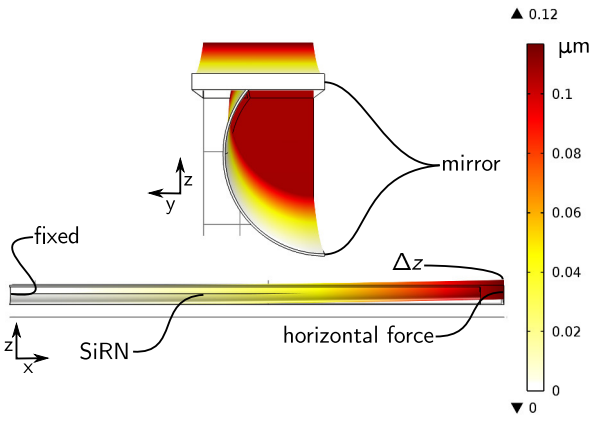

Fig. 4. Illustration of the finite element simulation with boundary conditions of the non-circularly shaped channel of 1000 µm. The color represents the displacement.

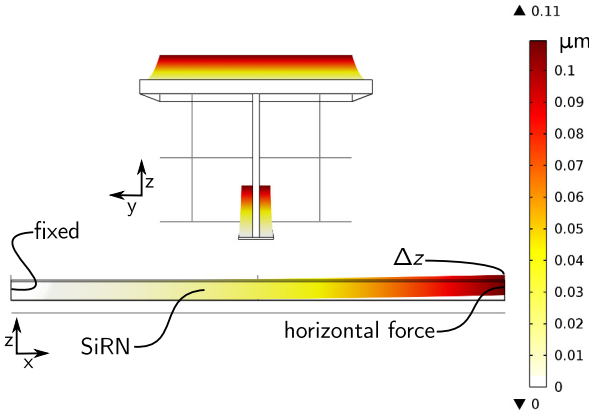

Fig. 5. Illustration of the finite element simulation with boundary conditions of the T-beam approximation with a length of of 1000 µm. The color represents the displacement.

B. Finite Element Models

The mechanics of the structure are also simulated using COMSOL Multiphysics 4.4 with the 'solid mechanics' physics. A non-circularly shaped channel is drawn using the dimensions in Table I. A custom material with the specified Young's modulus is used to model the silicon rich silicon nitride. To reduce simulation time and memory usage, only half of the structure is simulated using a 'mirror' boundary. A force, corresponding to a pressure of 1 bar at the surface, is applied at the end of the channel. The length of the channel is parameterized and swept from 600 µm to 3000 µm. Figure 4 shows an illustration of the 3D-structure with the boundary conditions.

To verify the T-beam approximation of the analytical model, a similar finite element simulation is done. In this simulation, a T-beam with the dimensions from Table I is drawn with the same material and same boundary conditions, but, since this structure needs less mesh elements, the mirror condition was not needed. Figure 5 shows an illustration of the structure with the boundary conditions.

The analytical model and both finite element models are combined with a capacitance model and are compared with measurement results below.

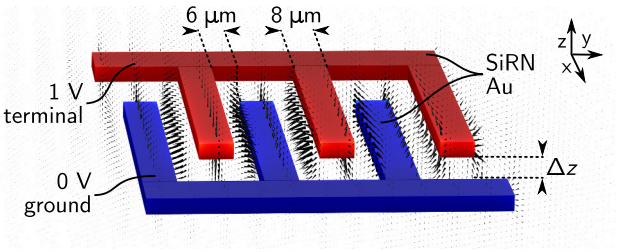

Fig. 6. Illustration of the finite element simulations of the electrostatic behavior of the electrodes. A summary of the boundary conditions, geometry and an impression of the result is shown. The resulting capacitances for different gaps $\Delta z(P)$ are plotted in Figure 7.

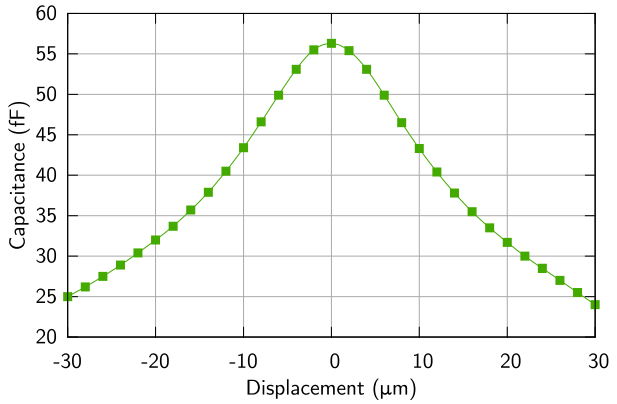

Fig. 7. Simulation results of the capacitance as a result of displacement, used as model $C_{\text{model}}(\Delta z(P))$.

C. Capacitance Model

The readout capacitor consists of two electrodes: one is attached to the tip of the structure and the other one is fixed. The capacitance is therefore a function of the displacement $\Delta z(P)$, and thus also a function of pressure.

The electrodes of the capacitor are comb-shaped and are simulated with COMSOL Multiphysics 4.4. With physics 'electrostatics', the capacitances for multiple electrode gaps, varying from −30 µm to 30 µm, are simulated (Figure 6).

The simulation results are shown in Figure 7. The results are interpolated and form the capacitive model $C_{\text{model}}(\Delta z(P))$.

D. Model Comparison

An initial displacement z_0 will be there due to internal stress from the fabrication process. This displacement is added as offset to the three mechanical models. From the mechanical models and the capacitance model, the capacitances for a pressure of 1 bar for the three models are calculated as a function of the length of the channel and are plotted in Figure 8.

The T-beam model is a reasonable approximation, since the results of both finite element simulations and the analytical model are very similar.

III. Integration With a Coriolis Mass Flow Sensor

As described above, out of plane bending of U-shaped non-circularly shaped channels can be read out statically to

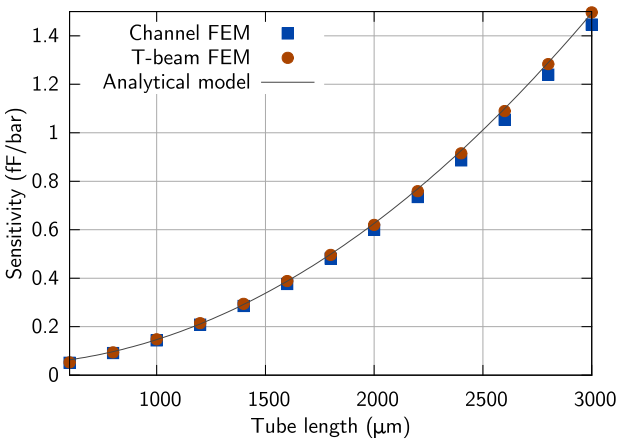

Fig. 8. Analytical result and finite element simulations of the scalability of the non-circularly shaped channel pressure sensors.

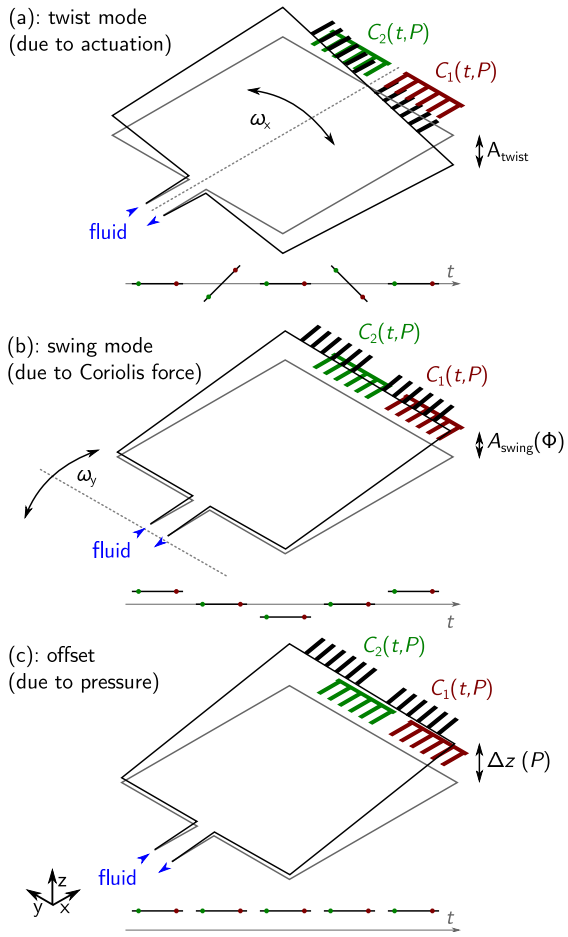

Fig. 9. Movement of a Coriolis mass flow sensor, with (a) the twist mode due to actuation, (b) the swing mode due to the Coriolis force and (c) the static offset due to the pressure.

obtain pressure information. However, actuating the suspended tubes makes flow and density measurement possible while the displacement can still be determined.

A. Coriolis Mass Flow Sensing

The structure of a Coriolis mass flow sensor [12], see Figure 9a, is very similar to the structure described above: a suspended channel with two capacitive readout structures.

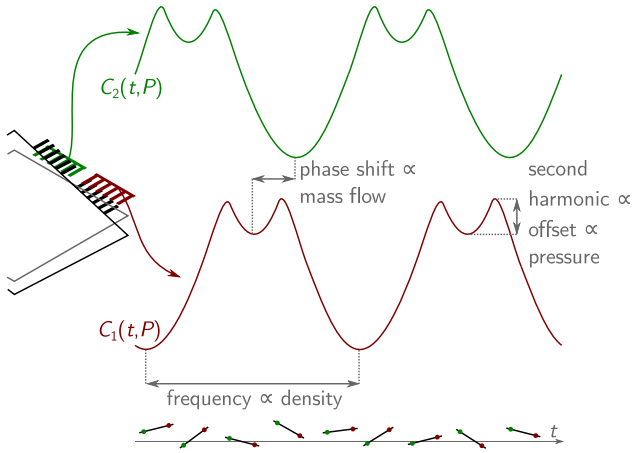

Fig. 10. The output signals of the Coriolis mass flow sensor: the phase shift is dependent on the mass flow, the frequency is dependent on the density and the ratio between the harmonics is dependent on the pressure.

By using a metal track on top of the channel with an alternating current in a magnetic field, the channel can be actuated at its resonance frqeuency in twist mode. When a fluid flows through the channel, Coriolis forces are induced that cause the channel to vibrate in swing mode (Figure 9b). The ratio between the two modes can be measured using two capacitive readout structures which produce the signals $C_1(t, P)$ and $C_2(t, P)$ as illustrated in Figure 10. The phase shift ϕ is related to this ratio, and thus, to mass flow [16]:

$$\phi \propto \arctan\left(\frac{A_{\text{swing}}}{A_{\text{twist}}}\right) \propto \arctan(\Phi), \tag{13}$$

with A_{swing} the amplitude of the swing mode, A_{twist} the amplitude of the twist mode and Φ the mass flow.

B. Resonator Based Density Sensing

The resonance frequency of the channel in twist mode (Figure 9a) is dependent on the moment of inertia of the tube with fluid inside and therefore also on the density of the fluid.

$$\omega_0 = \sqrt{\frac{k}{I_{\text{channel}} + I_{\text{fluid}}}} \propto \frac{1}{\sqrt{\rho_{\text{fluid}}}}, \tag{14}$$

with ω_0 the resonance frequency, k the torsional stiffness of the channel window, I_{channel} the moment of inertia of the channel window, I_{fluid} the moment of inertia of the fluid inside the channel window and ρ_{fluid} the density of the fluid. Hence, the resonance frequency of $C_1(t, P)$ and $C_2(t, P)$ is a measure for the density of the fluid [10].

C. Pressure Sensing

Since this structure is similar to the non-circularly shaped channel pressure sensor, it can be used for pressure sensing by measuring the offset (Figure 9c) of $C_1(t, P)$ and $C_2(t, P)$.

When one side of the readout structures is considered, the following equation describes the capacitance $C_{1|2}(t, P)$ of the moving comb.

$$C_{1|2}(t, P) = C_{\text{model}}(z_{1|2}(t, P)), \tag{15}$$

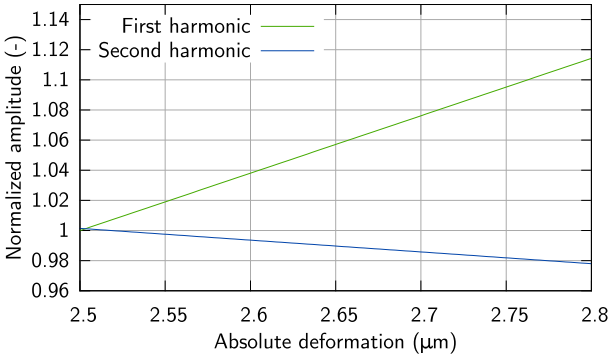

Fig. 11. The normalized amplitudes of the first two harmonics of the Coriolis mass flow sensor as a result of the displacement. Calculated from the analytical model.

where $C_{\text{model}}(z_{1|2}(t, P))$ is the capacitance as a function of position as plotted in Figure 7, and the position $z_{1|2}(t, P)$ is given by:

$$z_{1|2}(t, P) = \Delta z(P) + z_0 + \mathrm{B} \sin\left(\omega t + \frac{\phi}{2}\right), \qquad (16)$$

with B a constant factor dependent on the Lorentz actuation and actuation current and z_0 a static displacement due to residual stress in the channel material. The capacitance increases with decreasing distance and decreases with increasing distance. A maximum in capacitance is reached when the combs cross eachother. This causes the introduction of higher harmonics in the signal, illustrated in Figure 10 and described in [10]. A larger offset $\Delta z(P)$, as a result of a higher pressure, leads to smaller higher harmonics. The amplitudes of the first two harmonics are found by discretization of the time-domain signal $C_{1|2}(t, P)$ and apply a fast Fourier transform (FFT). Figure 11 shows the magnitudes of the first two harmonics for multiple absolute displacements $\Delta z(P) + z_0$.

The Coriolis mass flow sensor has two combs for phase detection. Both provide a set of harmonics which are dependent on the pressure. The pressure at both comb positions are different when there is a flow, since the channel between the combs has a pressure drop. This effect may be used as a ΔP flow sensor, like has been done in [17].

IV. Fabrication

The fabrication is based on the surface channel technology presented in [10]. Approximately 1 µm of silicon rich silicon nitride is deposited on a silicon-on-insulator wafer by low pressure chemical vapor deposition (Figure 12b). Then, the inlets and outlets are etched in the handle layer (400 µm) using deep reactive ion etching (Figure 12c).

A slit pattern is etched in the silicon rich silicon nitride layer on top of the wafer (Figure 12d). Using isotropic plasma etching with SF_6, channel molds (diameter of 40 µm) are formed under the slit pattern (Figure 12e). With wet etching using 50 % HF, the oxide layer between the channels and the inlets is etched (Figure 12f). A second deposition step of silicon rich silicon nitride is performed to form the channel walls and seal the slit pattern (Figure 12g).

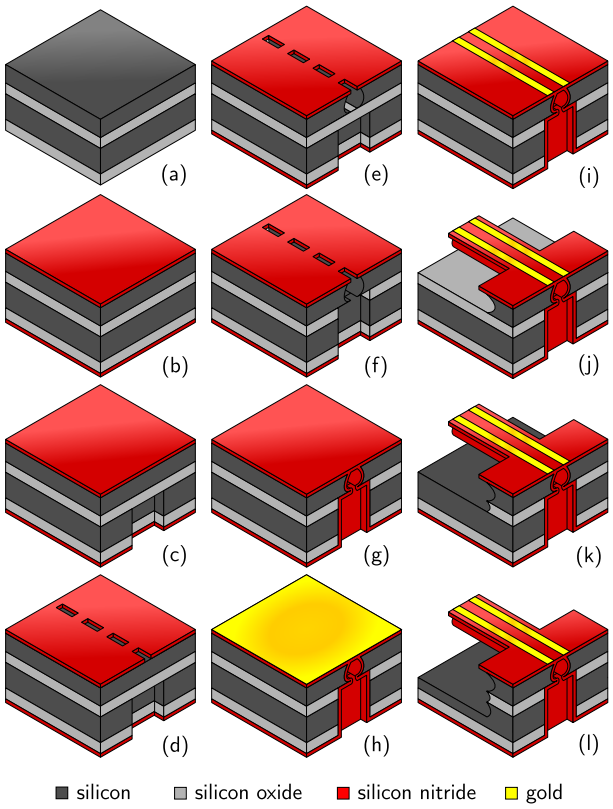

Fig. 12. Fabrication using surface channel technology in a silicon-on-insulator wafer (a), with (b) silicon nitride deposition, (c) backside inlet etching, (d) slits etching in the silicon nitride, (e) channel mold etching, (f) buried oxide layer etching, (g) silicon nitride deposition, (h) Cr/Au sputtering and (i) etching, (j), (k) and (l) release etching.

For the electrodes, 15 nm of Cr and 200 nm of Au are sputtered on the wafer (Figure 12h). The patterns are made with reactive ion beam etching (Figure 12i).

Isotropic plasma etching with SF_6 was used to etch around the channels (Figure 12j). A vapor phase HF etch released the channels from the silicon of the handle layer (Figure 12k) and another SF_6 plasma etch is used to provide more room for movement (Figure 12l).

V. Characterization

Two experiments are conducted:

- a static (without AC-actuation and flow) characterization of the pressure sensing mechanisms to validate the model and compare sensitivities (Figure 13) and
- a dynamic (with AC-actuation and flow) characterization to validate the possibility of simultaneous pressure and flow sensing and investigate crosstalk (Figure 14).

The static experiment is done with all sensors in Figure 15: the tubes with a length of 1000 µm, 1750 µm, 2500 µm. The dynamic measurements are done with the micro Coriolis mass flow sensor.

A. Static Experiment

Three sensors are characterized by applying a gauge pressure with nitrogen between 0 bar and 1 bar using a pressure

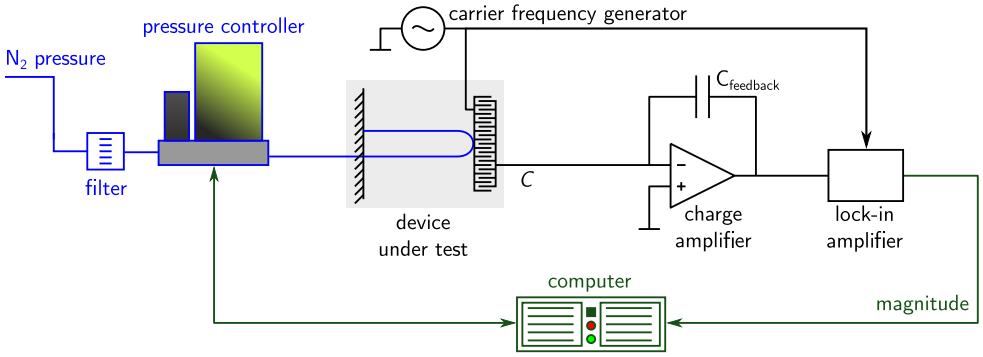

Fig. 13. Measurement setup for static characterization. A N_2 pressure is applied at the sensor using a pressure controller. The capacitive readout of the sensor is done using a carrier frequency fed to the capacitive readout structure of the sensor. A charge amplifier converted the capacitance to a voltage, which is demodulated using a lock-in amplifier.

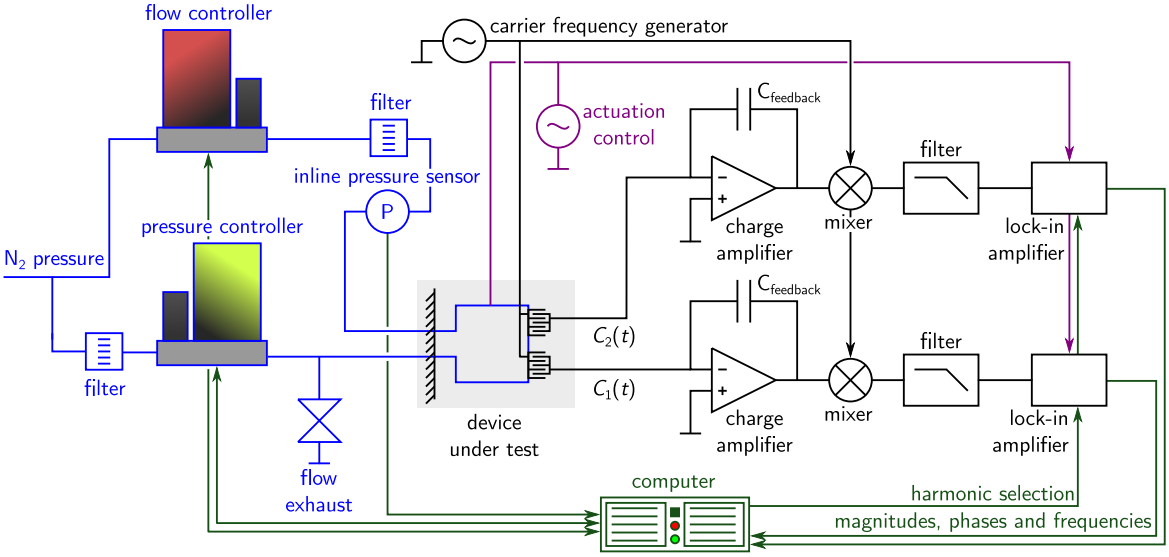

Fig. 14. Measurement setup for dynamic characterization. A N_2 flow is controlled at the inlet of the sensor and a pressure is controlled at the outlet of the sensor. A pressure sensor measures also the pressure at the inlet. The sensor is actuated using an actuation controller at its resonance frequency. The capacitive sensing is done similar to the static measurement. But in this situation, custom built electronics were used to do the demodulation and lock-in amplifiers (on the actuation frequency) were used to measure the magnitudes, phases and frequencies of the two readout signals corresponding to the capacitance values.

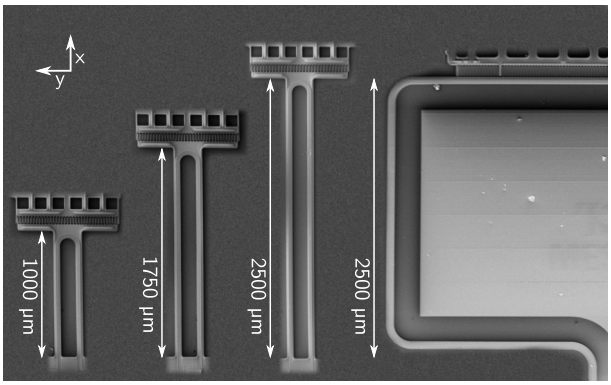

Fig. 15. Scanning electron microscopy image collage of the three different non-circularly shaped channel pressure sensors used in the experiments.

controller (Bronkhorst EL-PRESS). The electrical readout is done using a charge amplifier to convert the capacitance to a voltage. A sine wave ($\sim 1 \times 10^4$ Hz, 1 V) is fed to the combs. A lock-in amplifier (Stanford Research Systems SR830) is used to lock in on the frequency and reduce environmental noise. A schematic diagram of the setup, including the electronic readout, is shown in Figure 13.

The measurement results are shown in Figure 16. Longer tubes result in higher sensitivities: 0.2 fF bar^{-1} for the 1000 µm tube, 0.4 fF bar^{-1} for the 2500 µm tube and 1 fF bar^{-1} for the 2500 µm tube. The calculated results from the analytical model are also plotted and correspond very well to the measurements.

B. Dynamic Experiment

The measurement setup for the dynamic experiment is printed in Figure 14. The gauge pressure at the outlet of the sensor is controlled between 0 bar and 1 bar in steps of 0.2 bar using a pressure controller and a valve. For each pressure step, the mass flow is varied from 0 mg h^{-1} to 35 mg h^{-1} using a flow controller (Bronkhorst EL-FLOW) at the inlet of the sensor. A reference pressure sensor is also in line with the flow at the inlet of the sensor.

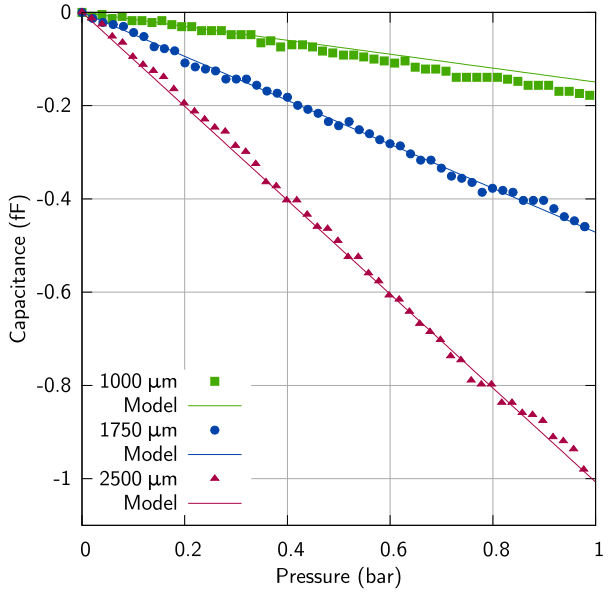

Fig. 16. Capacitive measurement results for gauge pressures from 0 bar to 1 bar for the different structures with lengths of 1000 µm, 1750 µm and 2500 µm. The results of the analytical model are also plotted.

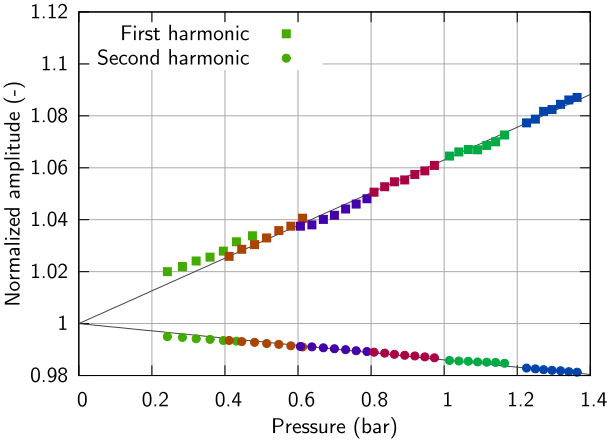

Fig. 17. Harmonics measurement for gauge pressures from 0 bar to 1.4 bar (measured by the inline pressure sensor) for the Coriolis mass flow sensor. The different colors represent the different pressure setpoints of the pressure controller.

The device under test is actuated by an actuation controller with feedback, which drives the sensor structure always exactly at the resonance frequency [10]. The capacitive measurement is done using a custom built circuit consisting of a charge amplifier and an analog lock-in amplifier (mixer/filter combination). Two commercially available lock-in amplifiers (Stanford Research Systems SR830) are used to lock-in on the actuation frequency and provide the amplitudes, phases and frequencies to a computer. For every unique flow and pressure combination, the amplitudes, phases and frequencies of both the first and second harmonic are obtained.

For increasing pressure, the first harmonic gains in amplitude while the second harmonic loses amplitude (Figure 17), as is predicted by the model. The pressure in the device under test is both dependent on the controlled pressure at the outlet and the controlled flow at the inlet, clearly visible in the results as increasing groups of points with the same color.

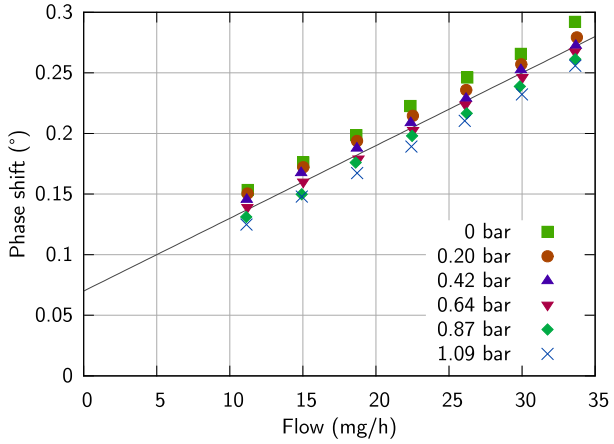

Fig. 18. Flow measurement for gauge pressures from 0 bar to 1 bar (measured by the pressure controller) for the Coriolis mass flow sensor.

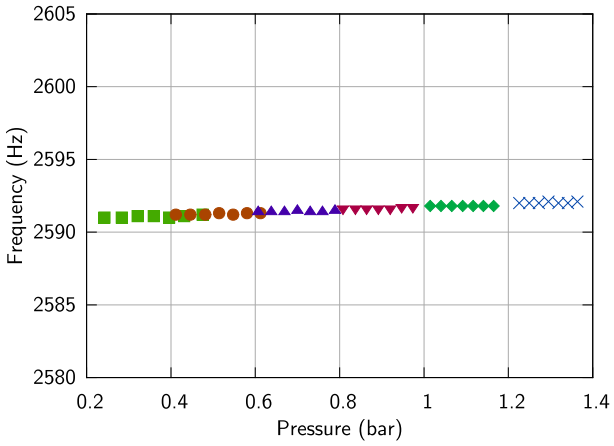

Fig. 19. Frequency measurement for gauge pressures from 0 bar to 1.4 bar (measured by the inline pressure sensor) for the Coriolis mass flow sensor.

The phase shift as a result of the flow is also measured and is shown in Figure 18. The resulted phase shift is also dependent on pressure.

Only nitrogen is used for the measurements, so no large differences in frequency as a result of the density are measured (Figure 19). A slightly increasing frequency as a function of pressure is observed. This may be caused by an increase in stiffness as a result of the displacement of the channel.

In Figure 20, the difference of the second harmonics between the two combs as a function of the flow is shown. This difference is proportional to the pressure drop between the two combs and is a measure for the flow, similar to how ΔP flow sensor operate.

The flow measurements of Figure 18 are corrected for the pressure dependence, using the information from the pressure measurement of Figure 17. The results are presented in Figure 21 and show how the proposed pressure sensing mechanism can significantly improve the reliability of the flow measurements.

VI. Discussion

The pressure sensing mechanism is completely integrated with the Coriolis mass flow sensor, hence, the design freedom

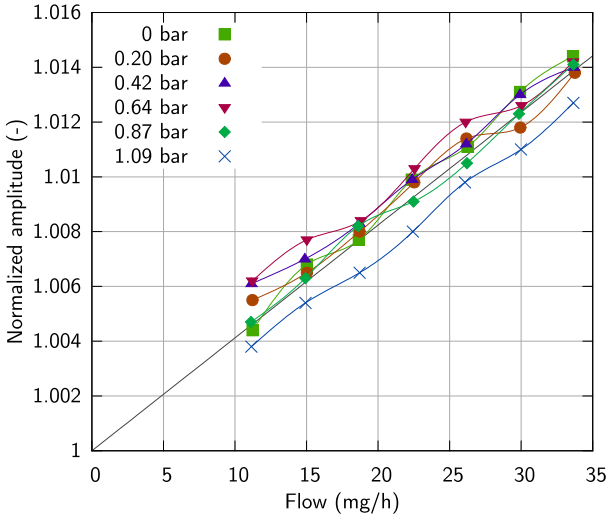

Fig. 20. Normalized amplitude of the difference of the second harmonic between the two combs for gauge pressures from 0 bar to 1 bar (measured by the pressure controller) plotted against mass flow.

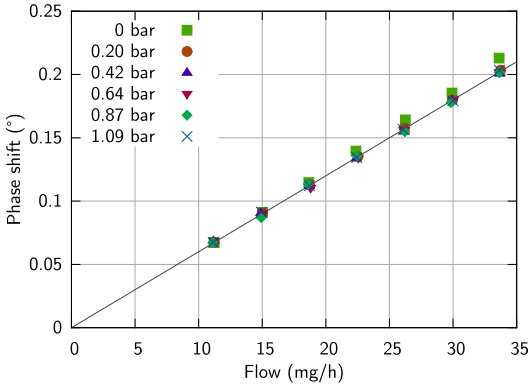

Fig. 21. Flow measurement based on the results of Figure 18 with pressure correction using the results of Figure 17. Corrected for offset.

is very limited. Therefore, the sensitivity is much lower than other capacitive pressure sensors in recently published articles [18], [19]. An improvement in performance can be achieved by including more capacitive readout structures around other positions at the tube, increasing the capacitance and enabling more accurate detection of the vibration modes.

We have not yet investigated the dependence of the pressure sensing mechanism on temperature. Temperature will also influence the residual stress and initial bending of the channel. Therefore, for accurate measurements temperature calibration will be necessary.

Both phenomena should be investigated in future work and both effects may be reduced by measuring differentially with a reference sensor which is actuated without flow. Also better results may be obtained when smart algorithms for sensor fusion are implemented.

VII. Conclusion

Micro channels that are fabricated using surface channel technology show a strong deformation caused by pressure. This non-ideal effect can be used for the integration of pressure sensors on a single-chip with a flow sensor. Three sensors with lengths of 1000 µm, 1750 µm and 2500 µm show sensitivites of 0.2 fF bar^{-1}, 0.4 fF bar^{-1} and 1 fF bar^{-1} respectively, and show good correspondence with the analytical model.

The same mechanism also influences the frequency spectrum of the capacitive output signals of a microfabricated Coriolis mass flow sensor, enabling the sensor to measure pressure in addition to mass flow and density without the need for any modifications to the sensor. Measurement of the pressure in a micro Coriolis flow sensor can also be used to compensate for pressure dependence of the sensor.

Acknowledgements

The authors gratefully acknowledge R. G. P. Sanders, J. Groenesteijn, and K. Ma for the technical help.

References

[1] S. Silvestri and E. Schena, "Micromachined flow sensors in biomedical applications," *Micromachines*, vol. 3, no. 2, pp. 225–243, 2012.
[2] G. M. Whitesides, "The origins and the future of microfluidics," *Nature*, vol. 442, no. 27, pp. 368–373, Jul. 2006.
[3] J. C. Lötters, J. Groenesteijn, E. J. van der Wouden, W. Sparreboom, T. S. J. Lammerink, and R. J. Wiegerink, "Fully integrated microfluidic measurement system for real-time determination of gas and liquid mixtures composition," in *Proc. 18th Int. Conf. Solid-State Sensors, Actuators, Microsyst. (TRANSDUCERS)*, Jun. 2015, pp. 1798–1801.
[4] P. E. Larsen, A. Boisen, and S. Schmid, "Hollow MEMS: An integrated sensor for combined density, viscosity, buoyant mass and IR absorption spectrometry," Ph.D. dissertation, Dept. Micro Nanotechnol., Techn. Univ. Denmark, Kongens Lyngby, Denmark, 2016.
[5] B. H. Jo, L. M. V. Lerberghe, K. M. Motsegood, and D. J. Beebe, "Three-dimensional micro-channel fabrication in polydimethylsiloxane (PDMS) elastomer," *J. Microelectromech. Syst.*, vol. 9, no. 1, pp. 76–81, Mar. 2000.
[6] Y.-J. Chuang, F.-G. Tseng, J.-H. Cheng, and W.-K. Lin, "A novel fabrication method of embedded micro-channels by using SU-8 thick-film photoresists," *Sens. Actuators A, Phys.*, vol. 103, no. 1, pp. 64–69, 2003.
[7] P. Enoksson, G. Stemme, and E. Stemme, "A silicon resonant sensor structure for Coriolis mass-flow measurements," *J. Microelectromech. Syst.*, vol. 6, no. 2, pp. 119–125, Jun. 1997.
[8] M. F. Khan, B. Knowles, C. R. Dennison, M. S. Ghoraishi, and T. Thundat, "Pressure modulated changes in resonance frequency of microchannel string resonators," *Appl. Phys. Lett.*, vol. 105, no. 1, p. 013507, 2014.
[9] R. W. Tjerkstra, M. De Boer, E. Berenschot, J. G. E. Gardeniers, A. van den Berg, and M. Elwenspoek, "Etching technology for microchannels," in *Proc. 10th Annu. Int. Workshop Micro Elect. Mech. Syst. (MEMS)*, Jan. 1997, pp. 147–152.
[10] J. Groenesteijn, "Microfluidic platform for coriolis-based sensor and actuator systems," Ph.D. dissertation, Dept. Elect. Eng., Math. Comput. Sci., Univ. Twente, Enschede, The Netherlands, Jan. 2016.
[11] M. Dijkstra, M. J. de Boer, J. W. Berenschot, T. S. J. Lammerink, R. J. Wiegerink, and M. Elwenspoek, "Miniaturized thermal flow sensor with planar-integrated sensor structures on semicircular surface channels," *Sens. Actuators A, Phys.*, vol. 143, no. 1, pp. 1–6, 2008.
[12] J. Haneveld *et al.*, "Modeling, design, fabrication and characterization of a micro coriolis mass flow sensor," *J. Micromech. Microeng.*, vol. 20, no. 12, p. 125001, 2010.
[13] D. Alveringh, J. Groenesteijn, R. J. Wiegerink, and J. C. Lötters, "Inline pressure sensing mechanisms enabling scalable range and sensitivity," in *Proc. IEEE 18th Int. Conf. Solid-State Sens., Actuators, Microsyst. (TRANSDUCERS)*, Jun. 2015, pp. 1187–1190.
[14] R. C. Hibbeler, *Statics and Mechanics of Materials*. Englewood Cliffs, NJ, USA: Prentice-Hall, 2004.
[15] A. Kaushik, H. Kahn, and A. H. Heuer, "Wafer-level mechanical characterization of silicon nitride MEMS," *J. Microelectromech. Syst.*, vol. 14, no. 2, pp. 359–367, 2005.

[16] D. Alveringh, J. Groenesteijn, R. J. Wiegerink, and J. C. Lötters, "Improved capacitive detection method for coriolis mass flow sensors enabling range/sensitivity tuning," *Microelectron. Eng.*, vol. 159, pp. 1–5, Jun. 2016.
[17] J. T. Suminto, G.-J. Yeh, T. M. Spear, and W. H. Ko, "Silicon diaphragm capacitive sensor for pressure flow acceleration and attitude measurements," in *Proc. 4th Int. Conf. Solid-State Sens. Actuators (TRANSDUCERS)*, Tokyo, Japan, 1987, pp. 336–339.
[18] Y. Zhang, R. Howver, B. Gogoi, and N. Yazdi, "A high-sensitive ultra-thin MEMS capacitive pressure sensor," in *Proc. 16th Int. Solid-State Sens., Actuators, Microsyst. Conf. (TRANSDUCERS)*, Jun. 2011, pp. 112–115.
[19] K. F. Lei, K.-F. Lee, and M.-Y. Lee, "Development of a flexible PDMS capacitive pressure sensor for plantar pressure measurement," *Microelectron. Eng.*, vol. 99, pp. 1–5, Nov. 2012.

Dennis Alveringh received the M.Sc. degree in electrical engineering from the University of Twente, Enschede, The Netherlands, in 2013, on the subject of a microfabricated multi-axis capacitive force/torque sensor. He joined the Micro Sensors and Systems Group, MESA+ Institute for Nanotechnology, University of Twente, where he is currently pursuing the Ph.D. degree in physical microfluidic sensors, e.g., noise limitations in Coriolis mass flow sensors, relative permittivity sensors, and pressure/flow sensor integration.

Remco J. Wiegerink received the M.Sc. degree in electrical engineering from the University of Twente, Enschede, The Netherlands, in 1988, on the subject of a fully integrated ultra-low frequency low-pass filter for offset canceling in integrated audio amplifiers, and the Ph.D. degree in electrical engineering from the University of Twente in 1992 on the subject of MOS translinear circuits. Between 1992 and 1995, he was in the Applied Physics Department, University of Twente, where he was engaged in the design of a superconducting flash analog-to-digital converter with GHz sampling frequency. In 1995, he joined the Transducer Science and Technology Group. Since then, his research has focused on mechanical microsensors, electronic interfacing of sensors, and packaging. Highlights include a silicon load cell with distributed capacitive readout, distributed thermal flow sensors using resistor arrays, an RF power sensor based on sensing the electrical force between the signal line, a suspended electrode, flow sensors based on the flow sensing hairs of crickets, and a micro-Coriolis flow sensor. He is currently the Head of the Micro Sensors and Systems Group, MESA+ Institute for Nanotechnology. He has authored or co-authored two books, *Analysis and Synthesis of MOS Translinear Circuits* and *Mechanical Microsensors*, and over 150 journal and conference papers. He has also co-authored several book chapters.

Joost C. Lötters received the M.Sc. degree in electrical engineering from the University of Twente, Enschede, The Netherlands, in 1993, on the subject of a buffer amplifier for a piezoelectric impact sensor, and the Ph.D. degree in electrical engineering from the University of Twente in 1997 on the subject of a highly symmetrical triaxial capacitive accelerometer. In 1997, he joined Bronkhorst High-Tech BV, Ruurlo, The Netherlands. Since then, his research has concentrated on flow measurement and control in the field of thermal and Coriolis flow sensing, including the ISO17025 accredited calibration laboratory. In 2010, he joined the Transducer Science and Technology Group, MESA+ Institute for Nanotechnology, University of Twente, as a part-time Associate Professor. Since then, his research has focused on microfluidic handling systems, i.e., integrated systems for the accurate measurement, control, dosage, and analysis of (micro) flows. Highlights include a micromachined thermal flow sensor using thermopiles, a micro-Coriolis flow sensor, a microproportional control valve, a micro-Wobbe index meter, and a single chip multiparameter flow measurement system comprising both a thermal and a Coriolis flow sensor, e.g., to determine the composition and energy content of gas mixtures. In 2015, he was appointed a part-time Professor of microfluidic handling systems with the University of Twente. He has invented or co-invented over 15 patents. He has authored or co-authored over 70 journal and conference papers. In 2013, he was appointed an Associate Editor-in-Chief of the *MDPI Journal of Micromachines*.